Rational Design of Layered Metal-Organic Framework Towards

High-Performance Adsorption of Hazardous Organic Dye

Dan-Dan Guo, Bo Li, Zhao-Peng Deng,[*] Li-Hua Huo and Shan Gao[*]

Key Laboratory of Functional Inorganic Material Chemistry, Ministry of Education, School

of Chemistry and Materials Science, Heilongjiang University, Harbin, 150080, People's

Republic of China

[*] Correspondence author E-mail: dengzhaopeng@hlju.edu.cn; shangao67@yahoo.com

Materials and Instruments

The size of activated carbon granule is 2~3 μm and the diameter of lamella graphene is 0.5~5 μm.

Infrared spectra (IR) were recorded from KBr pellets in the range of 4000-400 cm^{-1} on a Bruker Equinox 55 FT-IR spectrometer. Luminescence spectra were measured on a Perkin Elmer LS 55 luminescence spectrometer. Elemental analyses were carried out on a Vario MICRO from Elementar Analysensysteme GmbH. The crystal structure of **L-MOF-1** was determined at 293K by Xcalibur Eos diffractometer of Rigaku Company of Japan, (Mo-Kα X-ray, λ = 0.71073 Å). Powder X-ray diffraction (PXRD) patterns were measured at 293 K on a Bruker D8 diffractometer (Cu-Kα1, λ = 1.54059 Å). The TG analysis was carried out on a Perkin Elmer TG/DTA 6300 thermal analyzer under flowing N_2 atmosphere, with a heating rate of 10 °C min^{-1}. The concentration of CR was determined by a Perkin Elmer Lambda 900 UV/vis Spectrophotometer. The pH value of the solution was measured by a PHS-2C pH meter (Shanghai, China). The Zeta potential of **L-MOF-1** material was acquired on a Bruker Haven Zeta PALS potentiometer. The microstructure of CR-loaded **L-MOF-1** was observed by transmission electron microscopy (TEM, JEOL-JEM-2010, Japan).
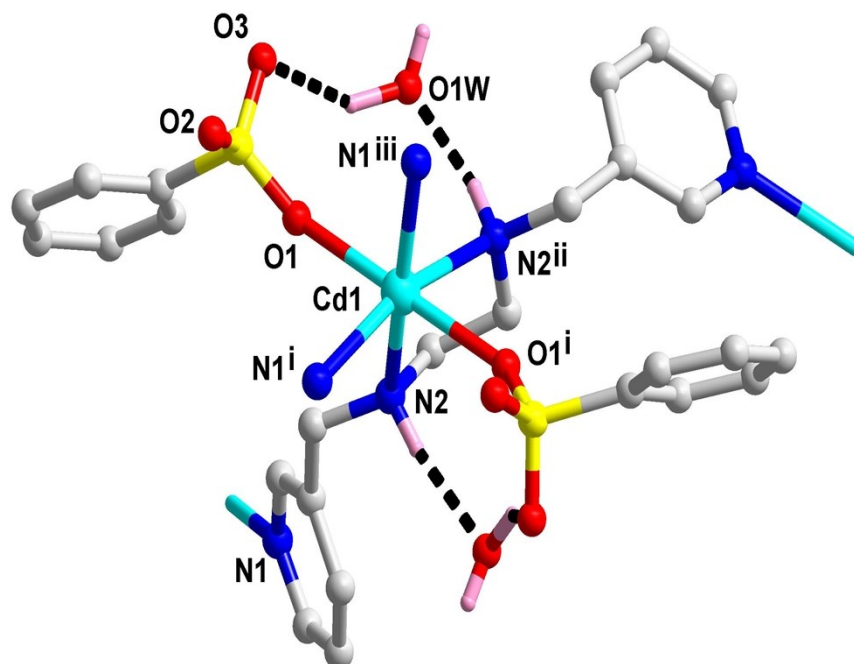
Fig. S1. Molecular structure of **L-MOF-1**.

X-ray crystallographic measurement

The diffraction data was collected at 295 K on a Xcalibur Eos diffractometer with graphite monochromatized Mo-$K\alpha$ (λ = 0.71073 Å) radiation in ω scan mode. The structure of **L-MOF-1** was solved by direct method and difference Fourier syntheses. All non-hydrogen atoms were refined by full-matrix least-squares technique on F^2 with anisotropic thermal parameters. The hydrogen atoms attached to carbons were placed in calculated positions with C–H = 0.93 (aromatic) and 0.97 (methelene) Å, and U (H) = 1.2U_{eq} (C) in the riding model approximation. The hydrogen atoms of water molecules and amino group were located in difference Fourier maps and were also refined in the riding model approximation, with O–H and N–H distance restraint (0.85(1) Å or 0.86(1) Å) and U(H) = 1.5U_{eq} (O,N). All calculations were carried out with the SHELXTL97 program. The CCDC reference number is 1851613. Crystal data, selected bond lengths and hydrogen bond parameters for **L-MOF-1** are listed as follows:

Empirical formula	$C_{26}H_{32}N_4O_8S_2Cd$
Formula weight	705.08
Space group	Orthorhombic
a/Å	12.2002(3)
b/Å	12.6969(3)
c/Å	18.9004(5)
α/°	90
β/°	90
γ/°	90
V/Å³	2927.74(12)
Z	4
D_c/g cm⁻³	1.600
μ (MoKα)/mm⁻¹	0.943
F(000)	1440
Reflections collected	6745
Unique reflections	3356
Parameters	195
R(int)	0.0263
GOF on F^2	1.034
Final R indices [$I \geq 2\sigma(I)$]	R1 = 0.0344, wR$_2$ = 0.0706

Hydrogen bond parameters for **L-MOF-1**				
D-H...A	d(D-H)/Å	d(H...A)/Å	d(D...A)/Å	<(DHA)/°
N(2)-H(2N1)...O(1W)#1	0.86(4)	2.111(12)	2.953(4)	168(3)
O(1W)-H(1W2)...O(3)#2	0.85(3)	1.987(17)	2.788(3)	158(3)

Symmetry transformations used to generate equivalent atoms: #1 -x+1/2,y-1/2,z; #2 -x,-y+2,-z+2

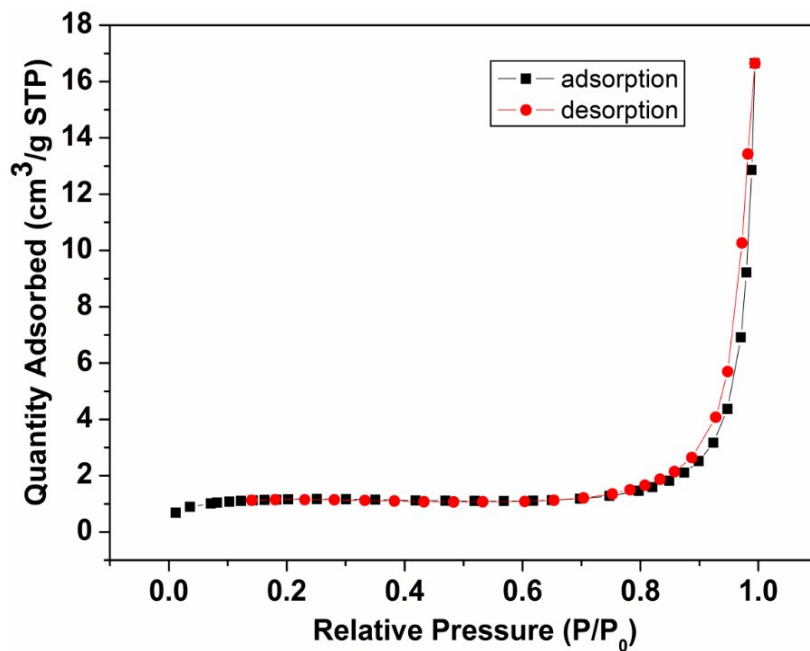| Selected bond lengths [Å] for **L-MOF-1**			
Cd(1)-N(1)#1	2.333(2)	Cd(1)-O(1)#1	2.353(2)
Cd(1)-N(1)	2.333(2)	Cd(1)-N(2)#2	2.372(2)
Cd(1)-O(1)	2.353(2)	Cd(1)-N(2)#3	2.372(2)

Fig. S2. Nitrogen adsorption–desorption isotherms of **L-MOF-1** material.
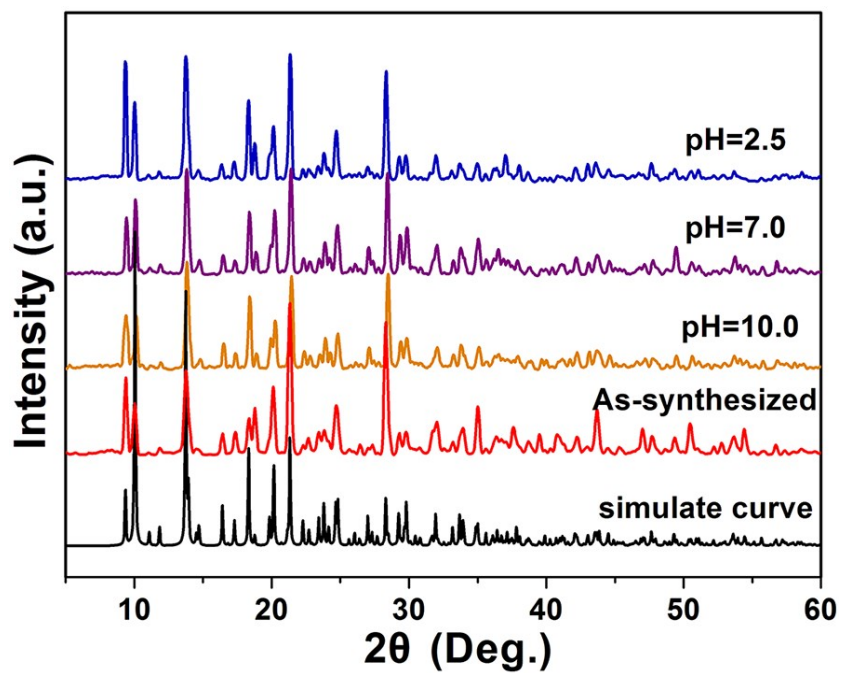

Fig. S3. XRD patterns of **L-MOF-1** and the samples after being soaked in aqueous solution at different pH values.

Thermal Stability of L-MOF-1

The TG curve in Fig. S4 shows that **L-MOF-1** loses the lattice water molecules between 75 and 150 °C (obsd. 4.80 %, calcd. 5.10 %). The following weight loss corresponds to the decomposition of organic parts in the range of 283-615°C with the final residual of cadmium sulfide (obsd. 20.36 %, calcd. 20.42 %). Therefore, it can be concluded from the TG results that the coordinated skeleton of **L-MOF-1** has good thermal stability, supporting for its use as adsorption material.
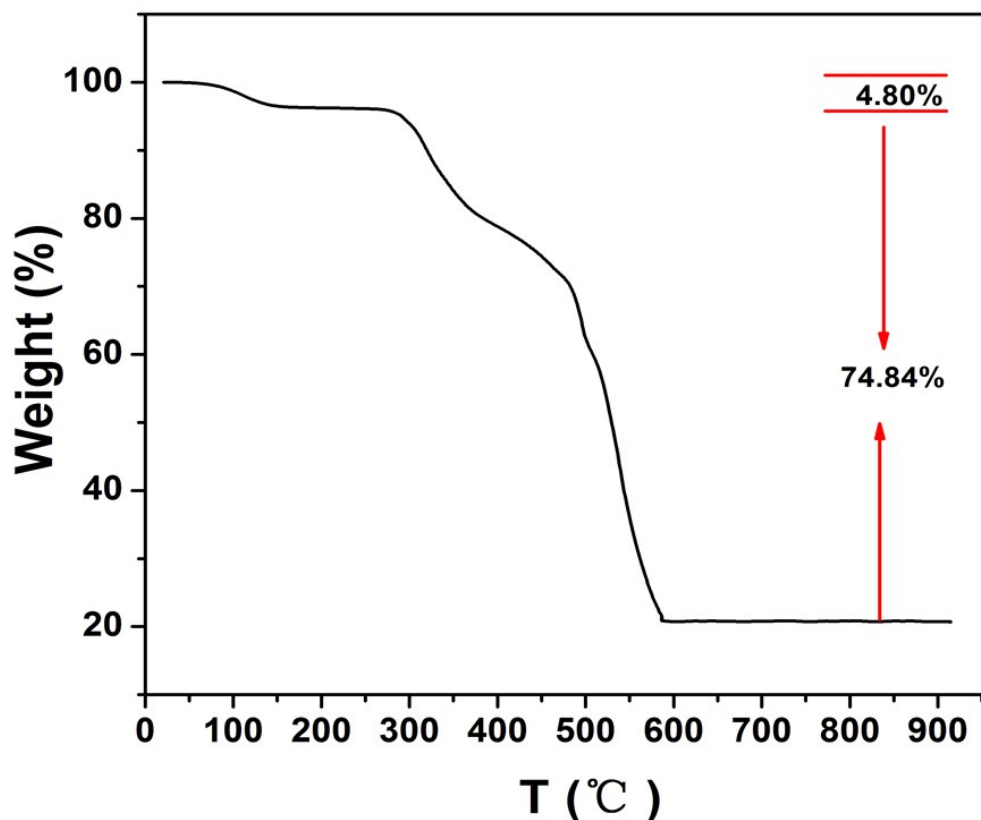

Fig. S4. TG curve of **L-MOF-1** under N_2 atmosphere.

Measurement of Zeta Potential

Equal amount of **L-MOF-1** (5 mg) was separately added to 5 mL aqueous solution with different pH value of 2.2, 3.0, 4.1, 5.0, 7.0, 8.8, 10.5 (the pH value of

the solution was adjusted by 0.10 mol·L^{-1} HCl and NaOH, and the pH value was detected by pH meter). After being ultrasound for 5 min, the Zeta potential was measured by Zeta potentiometer.

Adsorption Experiments

Different concentrations (100-2300 mg·L^{-1}) of CR solution (100 mL) were separately placed in 250 mL iodine flask. Then, 10 mg **L-MOF-1** was added to each bottle followed by stirring at room temperature. At different time intervals, 4 mL mixture of the suspension was taken from the reaction system and centrifuged at 8000 rpm for 2 min to remove the solid samples. The concentrations of the left solution were monitored by a UV-vis spectrophotometer. The characteristic absorption peaks of CR at 499 nm (pH = 5.0~12.0) and 580 nm (pH = 2.0~5.0) were chosen to supervise the adsorption process.

Adsorption Kinetics

Equal amount of **L-MOF-1** (10 mg) was separately added to 100 mL different concentration of CR aqueous solution (300, 700 and 1200 mg·L^{-1}, pH value is about 3.0). The kinetics of the adsorption process was determined according to the same method in adsorption experiments. The kinetics of CR adsorption by **L-MOF-1** was described by pseudo-first-order[1] and pseudo-second-order[2] kinetic rate equations.

The pseudo-first-order kinetics:

$$\log(q_e - q_t) = \log q_e - \frac{k_1}{2.303}t$$

(1)

The pseudo-second-order kinetics:

$$\frac{t}{q_t} = \frac{1}{k_2 q_e} + \frac{1}{q_e} t \qquad (2)$$

where q_e is equilibrium adsorption capacity (mg·g⁻¹); q_t is adsorption capacity at time t (mg·g⁻¹), t is adsorption time (min), k_1 is the first order kinetic constant, k_2 is the second order kinetic constant.

Adsorption Isotherms

Equal amount of **L-MOF-1** (10 mg) was separately added to 100 mL different concentration of CR aqueous solution (300-1300 mg·L⁻¹, pH value is about 3.0). The equilibrium CR concentration after adsorption in each system was measured to calculate the equilibrium adsorption capacity. The experimental approaches were carried out as described above. The adsorption isotherms were fitted with Langmuir and Freundlich models[3,4].

Langmuir model:

$$q_e = \frac{q_m K_L C_e}{1 + K_L C_e} \qquad (3)$$

Freundlich model:

$$q_e = K_f C_e^{1/n} \qquad (4)$$

where C_e is equilibrium concentration of CR (mol·L⁻¹), q_e (mg·g⁻¹) is equilibrium

adsorption capacity; q_m (mg·g^{-1}) represents the maximum adsorption capacity; K_L and K_f are Langmuir constant and Freundlich constant, respectively; n represents the strength of the driving force of adsorption.

The favorability of an adsorption system can also be expressed in terms of a dimensionless separation factor (R_L) shown below[5]:

$$R_L = \frac{1}{1 + C_m K_L} \tag{5}$$

where C_m is the maximum initial concentration of CR; K_L is the Langmuir constant.

Adsorption Thermodynamics

The equilibrium adsorption capacity and equilibrium concentration of CR were obtained by adding 10 mg **L-MOF-1** to 100 mL different concentrations of CR aqueous solution (300-2300 mg·L^{-1}, pH value is about 3.0). The experimental approaches were carried out as described above. The thermodynamic data were obtained by fitting the measured data under 293, 303 and 313 K by Langmuir model.

Gibbs free energy equation[6]:

$$\Delta G = -RT \ln K_L \tag{6}$$

The enthalpy change (ΔH) and entropy change (ΔS) were calculated from the Van't Hoff's equation[7]:

$$\ln K_L = \frac{\Delta S}{R} - \frac{\Delta H}{RT} \tag{7}$$

where ΔG is the Gibbs free energy; K_L is the Langmuir constant ($L \cdot mol^{-1}$); T is the absolute temperature (K); R is the universal gas constant (8.314 $J \cdot mol^{-1} \cdot K^{-1}$). The values of enthalpy change ΔH ($KJ \cdot mol^{-1}$) and entropy change ΔS ($J \cdot mol^{-1} \cdot K^{-1}$) were calculated from the slope ($-\Delta H/R$) and the intercept ($\Delta S/R$) of a linear plot of lnK_L versus $1/T$, respectively.
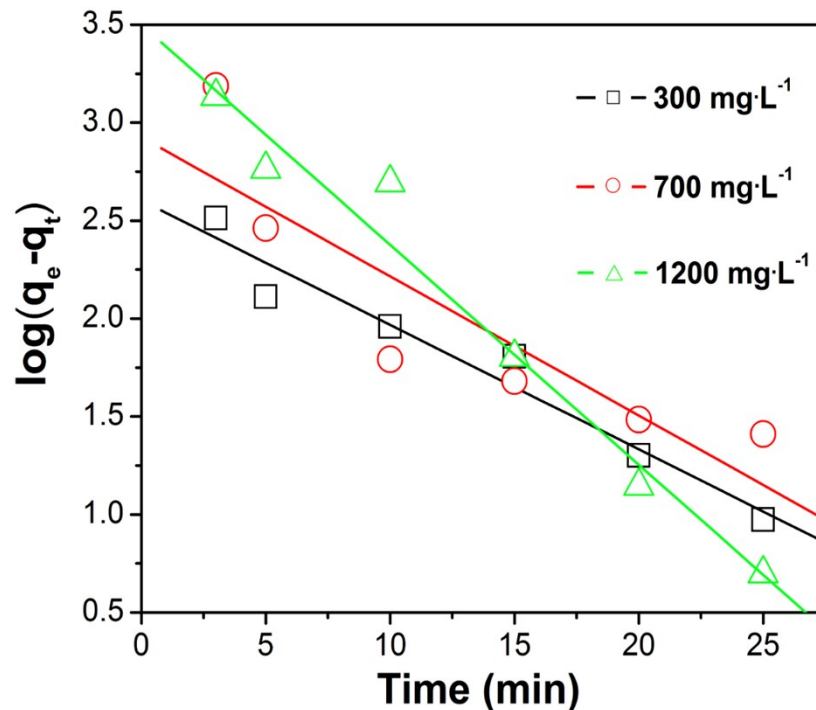

Fig. S5. Plots of pseudo-first-order kinetics.

References

1. S. Lagergren, *K Sven Vetenskapsakad Handl,* 1898, **24**, 1–39.

2. Y. S. Ho and G. McKay, *Chem. Eng. J.,* 1998, **70**, 115–124.

3. I. Langmuir, *J. Am. Chem. Soc.,* 1916, **38**, 2221–2295.

4. H. M. F. Freundlich, *Z. Phys. Chem.,* 1906, **57**, 385–471.

5. J. H. Huang, K. L. Huang, S. Q. Liu, A. T. Wang and C. Yan, *Colloid Surf. A: Physicochem. Eng. Aspects,* 2008, **330**, 55–61.

6. T. W. Weber and R. K. Chakkravort, *AIChE J.,* 1974, **20**, 228–238.

7. X. J. Jia, J. S. Wang, J. S. Wu, Y. C. Du, B. X. Zhao and D. den Engelsen, *RSC Adv.,* 2015, **5**, 72321–72330.
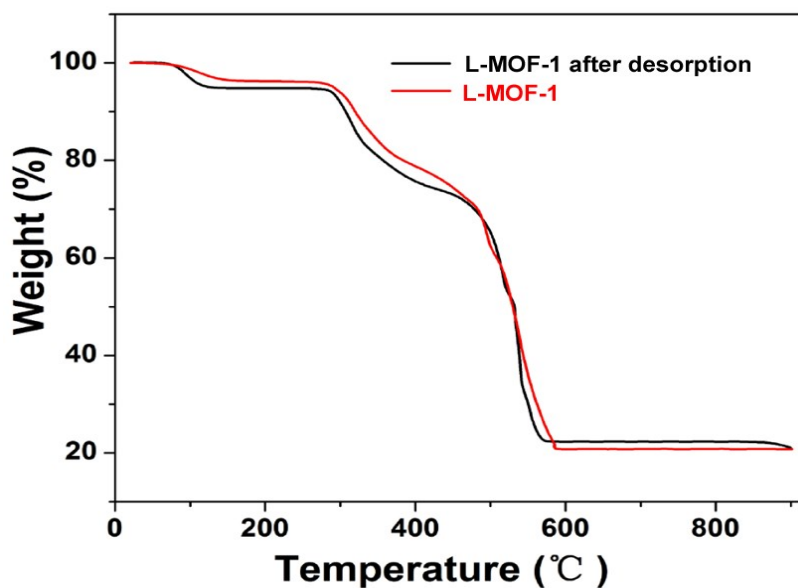
Fig. S6. TG curves of **L-MOF-1** and **L-MOF-1** after desorption and washing.
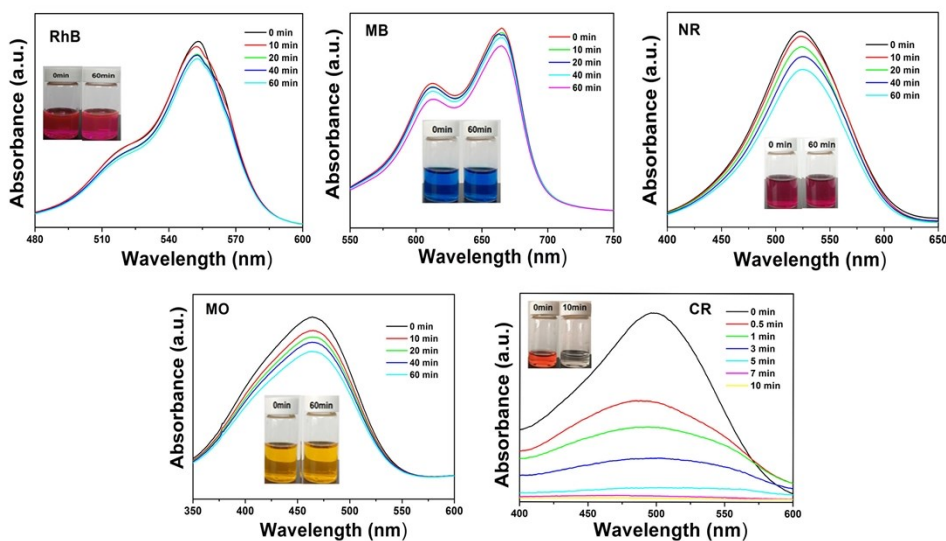

Fig. S7. UV-vis adsorption spectra of different dyes in aqueous solution with addition of 10 mg **L-MOF-1** absorbent.
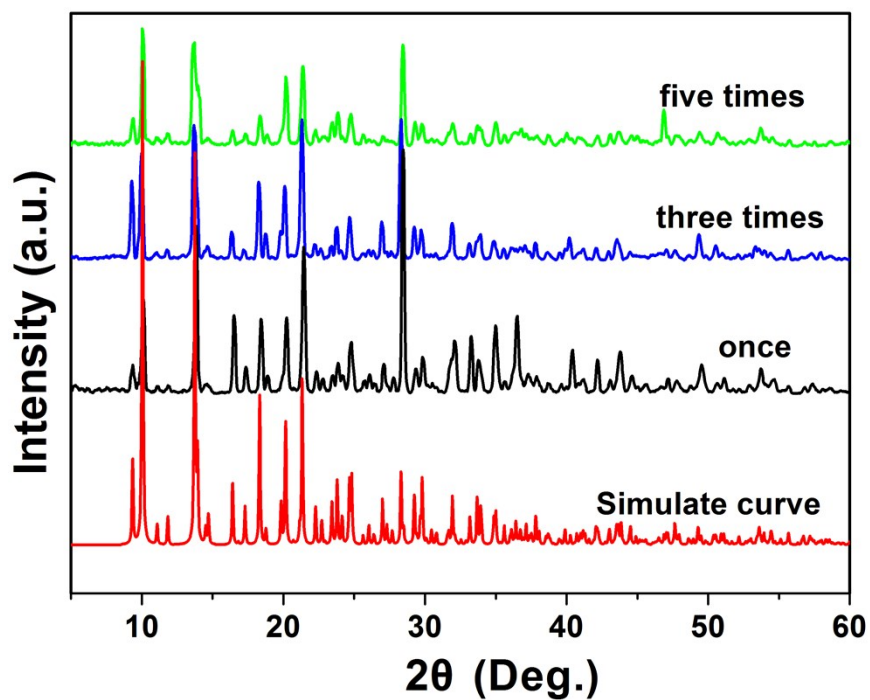
Fig. S8. PXRD patterns of **L-MOF-1** after desorption and washing.

Table S1. Comparison of the maximum adsorption capacity and contact time of different adsorbents

towards CR dye[a]

adsorbents	Structure	q_m (mg·g^{-1})	Contact time (min)	References
$[Cd(H_2L)(BS)_2]_n \cdot 2nH_2O$ (**L-MOF-1**)	2-D	12314	20	This work
$[Co_3(tib)_2(H_2O)_{12}](SO_4)_3$ (BUC-17)	2-D	4923.7	3	1
$[Cu(bipy)(SO_4)]_n$	1-D	2429	60	2
$[Cd(L1)]$	2-D	1374.68	180	3
$[In(OH)(BDC)]_n \cdot nDMF \cdot nH_2O$ [MIL-68 (In)]	3-D	1204	60	4
$[Ni_{1.5}Cu_{1.5}(BTC)_2]_n$	3-D	1100	--	5
$[Co(L2)(BDC)]_n$	1-D	928.4	1440	6
$\{[Ag(abtz)] \cdot (NO_3) \cdot (0.125H_2O)\}_n$	1-D	823	1440	7

$[Fe_3O(H_2O)_2(F)(BTC)_2]_n$·14.5n$H_2O$ [MIL-100(Fe)]	3-D	714	400	8
$Cd_4(H_4L3)_2(phen)_2(H_2O)_4$	3-D	684	60	9
{[$Cu_3(btb)_3(nbta)_2$]·($H_2O)_2$}$_n$	3-D	642	1440	10
{[$CdCl_2(L4)$]}$_n$	2-D	485.4	--	11
[$Co(mim)_2$]$_n$ (ZIF-67)	3-D	402.5	--	12
MgO/SiO_2 Composites	Particle	4000	150	13
Rod-like MgO	Porous	3236	90	14
ZnAl-LDO-3	Layered	1540	360	15
α-Fe/Fe_3O_4 composite	Lamellar	1297	3	16
Polyaniline/Fe^0 composite	nanofibers	1150	60	17
Activated carbon (AC)	Porous	376	180	18

[a] H_2L = N1,N2-bis(pyridin-3-ylmethyl)ethane-1,2-diamine, HBS = benzenesulfonic acid; H_2L1 = 5-(3,5-dimethyl-1H-pyrazol-1-yl) 1,3-benzene-dicarboxylic acid; H_2BDC = benzenedicarboxylic acid; H_3BTC = 1,3,5-benzenetricarboxylic acid; L2 = 1,3-bis(5,6-dimethylbenzimidazole)propane; abtz = 1-(4-aminobenzyl)-1,2,4-tri azole; H_8L3 = tetraphenylsilane tetrakis-4-phosphonic acid; btb = 4,4'-bis (1,2,4-triazolyl-1-yl)-biphenyl; H_3nbta = 5-nitro-1,2,3-benzenetricarboxylic acid; L4 = 1,2,3,4,5-pentasubstituted cyclohexanol; Hmim = 2-methylimidazole.

Table S2. Adsorption parameters of isotherm for the adsorption of CR on **L-MOF-1**.

Langmuir				Freundlich		
q_m (mg·g^{-1})	K_L	R^2		Kf	n	R^2
12314	0.62	0.99		7946	9.689	0.77

References

1. J.-J. Li, C.-C. Wang, H.-f. Fu, J.-R. Cui, P. Xu, J. Guo and J.-R. Li, *Dalton Trans.,* 2017, **46**, 10197–10201.

2. L. Xiao, Y. Xiong, S. H. Tian, C. Q He, X. Su and Z. H. Wen, *Chem. Eng. J.,* 2015, **265**,

157–163.

3. N. Kumar and A. K. Paul, *Inorg. Chem.,* 2020, **59**, 1284–1294.

4. L. N. Jin, X. Y. Qian, J. G. Wang, H. Aslan and M. D. Dong, *J. Colloid Interf. Sci.,* 2015, **453**, 270-275.

5. J. Hu, H. Yu, W. Dai, X. Yan, X. Hu and H. Huang, *RSC Adv.,* 2014, **4**, 35124–35130.

6. S. L. Xiao, Y. H. Li, P. J. Ma and G. H. Cui, *Inorg. Chem. Commun.,* 2013, **37**, 54–58.

7. B. Ding, C. Guo, S. X. Liu, Y. Cheng, X. X. Wu, X. M. Su, Y. Y. Liu and Y. Li, *RSC Adv.,* 2016, **6**, 33888–33900.

8. S. E. Moradia, S. Dadfarniaa, A. M. H. Shabania and S. Emamib, *Desalin. Water Treat.,* 2014, **52**, 1–13.

9. J. Ai, H.-R. Tian, X. Min, Z.-C. Wang and Z.-M. Sun, *Dalton Trans.,* 2020, **49**, 3700–3705.

10. X. X. Wang, Z. X. Li, B. Y. Yu, K. H. Van and G. H. Cui, *Inorg. Chem. Commun.,* 2015, **54**, 9–11.

11. W. Xu, Z. Shao, C. Huang, R. Xu, B. Dong and H. Hou, *Inorg. Chem.,* 2019, **58**, 3959–3967.

12. X. D. Du, C. C. Wang, J. G. Liu, X. D. Zhao and P. Wang, *J. Colloid Interf. Sci.,* 2017, **506**, 437–441.

13. M. Q. Hu, X. L. Yan, X. Y. Hu, J. J. Zhang, R. Feng and M. Zhou, *J. Colloid Inter. Sci.,* 2018, **510**, 111–117.

14. Z. Q. Bai, Y. J. Zheng and Z. P. Zhang, *J. Mater. Chem. A,* 2017, **5**, 6630–6637.

15. G. L. Huang, Y. Y. Sun, C. C. Zhao, Y. F. Zhao, Z. Y. Song, J. L. Chen, S. L. Ma, J. P. Du and Z. G. Yin, *J. Colloid. Inter. Sci.,* 2017, **494**, 215–222.

16. L. X. Wang, J. C. Li, Z. T. Wang, L. J. Zhao and Q. Jiang, *Dalton Trans.,* 2013, **42**, 2572–2579.

17. X. J. Jia, J. S. Wang, J. S. Wu, Y. C. Du, B. X. Zhao and D. den Engelsen, *RSC Adv.,* 2015, **5**, 72321–72330.

18. M. K. Purkait, A. Maiti, S. DasGupta and S. De, *J. Hazard. Mater.,* 2007, **145**, 287–295.